Influence of Landau-level mixing on Wigner crystallization in graphene

C.-H. Zhang and Yogesh N. Joglekar
Department of Physics, Indiana University-Purdue University Indianapolis, Indianapolis, Indiana 46202, USA
(Received 27 February 2008; revised manuscript received 21 April 2008; published 19 May 2008)

Graphene, with its massless linearly dispersing carriers, in the quantum Hall regime provides an instructive comparison to conventional two-dimensional systems in which carriers have a nonzero band mass and quadratic dispersion. We investigate the influence of Landau-level mixing in graphene on Wigner crystal states in the nth Landau level obtained using single-Landau-level approximation. We show that the Landau-level mixing does not qualitatively change the phase diagram as a function of partial filling factor ν in the nth level. We find that the inter-Landau-level mixing, which is quantified by relative occupations of the two Landau levels, ρ_{n+1}/ρ_n, oscillates around 2% and, in general, remains small (<4%) irrespective of the Landau-level index n. Our results show that the single-Landau-level approximation is applicable in high Landau levels, even though the energy gap between the adjacent Landau levels vanishes.

DOI: 10.1103/PhysRevB.77.205426 PACS number(s): 73.43.−f, 73.20.Qt

I. INTRODUCTION

Wigner crystallization, where the density profile of carriers in a system spontaneously develops a periodic spatial modulation, is a classic example of the interplay between (classical) repulsive potential energy and (quantum) kinetic energy associated with the localization of carriers as the density of carriers is varied.[1–3] Although predicted in 1934,[1] this phenomenon has defied direct experimental observation in bulk systems and conventional two-dimensional (2D) systems. In quantum Hall systems, where the kinetic energy of carriers is quantized and quenched, Wigner crystallization is induced by a competition between the electrostatic and exchange interactions as the partial filling factor ν in a given Landau level is varied. (In the quantum Hall regime, Wigner crystallization depends only on the filling factor and can occur at any carrier density.[4]) Wigner crystallization in the lowest Landau level has been inferred via transport measurements,[5] and the anisotropic transport observed[6] in high Landau levels can be interpreted[7] in terms of anisotropic Wigner crystal ground states. A direct observation of the Wigner crystal via local carrier density, however, has not yet been possible. Graphene, with its massless carriers on the surface, is a unique and ideal candidate for this purpose.[8,9] Recent studies using Hartree–Fock mean-field theory in the single-Landau-level approximation[10] (SLLA) or exact diagonalization in the single-Landau-level subspace[11] have predicted that Wigner crystal states will appear as ground states over a range of partial filling factor ν in a given Landau level. In this paper, we examine the validity of the single-Landau-level approximation.

Let us first recall the relevant results for a conventional 2D system in a perpendicular magnetic field B with a partial filling factor of $\nu \leq 1$ in the Landau level n. Thus, the actual filling factor for spinless carriers (with no other degeneracies) is $n+\nu$. For this system, the difference between energies of the adjacent Landau levels is $\Delta E_n = E_{n+1} - E_n = \hbar\omega_c$, where $\omega_c = eB/mc$ is the cyclotron frequency and m is the band mass of the carriers.[12] We remind the reader that $\Delta E_n = \hbar^2/ml_B^2$ is (approximately) the quantum kinetic energy of a particle with mass m in a box with size $l_B = \sqrt{\hbar c/eB}$. The Coulomb interaction that causes transitions between different Landau levels has a typical energy scale of $V_c = e^2/\epsilon l_B$, where $\epsilon \sim 10$ is the dielectric constant (for gallium arsenide). Therefore, the ratio of these two energy scales is $V_c/\Delta E_n = l_B/a_B$, where $a_B = \hbar^2\epsilon/me^2$ is the Bohr radius of the carriers in the material. Since a_B is independent of the magnetic field and the magnetic length $l_B \propto 1/\sqrt{B}$, as $B \to \infty$, the amplitude for inter-Landau-level transitions vanishes and the SLLA becomes a good approximation.[13] A corresponding analysis for graphene shows the stark difference between the two systems. The gap between the adjacent Landau-level energies in graphene is $\Delta E_n = E_{n+1} - E_n = \hbar\omega[\sqrt{2(n+1)} - \sqrt{2n}]$, where $\omega = v_G/l_B$ is the cyclotron frequency, $v_G \sim c/300$ is the speed of massless carriers in graphene, and c is the speed of light. It follows that the ratio

$$g_n = \frac{V_c}{\Delta E_n} = \frac{e^2}{\epsilon\hbar v_G}\frac{1}{\sqrt{2(n+1)} - \sqrt{2n}} \tag{1}$$

is independent of the magnetic field and diverges, $g_n \sim \sqrt{2n}$, as $n \to \infty$. Based on this naive analysis, we would expect that the inter-Landau-level transitions become increasingly important as the Landau-level index n increases, irrespective of the magnetic field; even in the lowest Landau level, the ratio $g \sim e^2/\epsilon\hbar v_G = \alpha_G \sim 1$ is not small (α_G is the fine structure constant for graphene). This analysis suggests that the SLLA is not reliable in graphene for any B and that it gets worse with increasing n since the energy gap $\Delta E_n \to 0$. We emphasize here that this naive analysis, as we will show below, is invalid. Indeed, the cyclotron radius of a particle in Landau level n is given by $R_c(n) = l_B\sqrt{2n+1}$, although the area per particle in a given Landau level is still $2\pi l_B^2$. Therefore, if we estimate the Coulomb energy as $\tilde{V}_c = e^2/\epsilon R_c(n) = V_c/\sqrt{2n+1}$, we find that $\tilde{g}_n = \tilde{V}_c/\Delta E_n$ becomes independent of n and the Landau-level mixing remains independent of the Landau-level index and the magnetic field.[14,15] In the following, we show that the effect of Landau-level mixing in graphene is small and SLLA is applicable.

The outline of the paper is as follows. In Sec. II, we briefly describe the Hartree–Fock approximation with Landau-level mixing and outline our approach. The details presented in this section are essentially identical to those in our earlier work.[10] In Sec. III, we present the results obtained without and with Landau-level mixing. We find that the Landau-level mixing does not qualitatively change the phase diagram of the system. We quantify the mixing using off-diagonal self-energy and relative occupation of Landau levels n and $n+1$. We compare the results for Landau level mixing as a function of n in graphene with those for conventional 2D systems. We summarize our conclusions in Sec. IV.

II. MICROSCOPIC HAMILTONIAN AND HARTREE–FOCK APPROXIMATION

Let us consider graphene in a strong perpendicular magnetic field B in the quantum Hall regime. The single-particle states of the noninteracting system are given by $|n,k,\sigma\rangle$, where (n,k) denote the Landau level and intra-Landau-level indices, and $\sigma=\pm$ correspond to the two inequivalent valleys $\mathbf{K}$ and $\mathbf{K}'=-\mathbf{K}$ in the Brillouin zone. The details presented in this section closely follow Ref. 10. The Hamiltonian for the system, including the Coulomb interaction is

$$\hat{H} = N_\phi \sum_{n\sigma} (E_n-\mu)\hat{\rho}^{\sigma,\sigma}_{n,n}(0) + \frac{1}{2A}\sum_{\sigma_i n_j \mathbf{q}} V(\mathbf{q})\mathcal{F}_{n_1,n_2}(-\mathbf{q}) \times \hat{\rho}^{\sigma_1,\sigma_1}_{n_1,n_2}(\mathbf{q})\mathcal{F}_{n_3,n_4}(-\mathbf{q})\hat{\rho}^{\sigma_3,\sigma_3}_{n_3,n_4}(\mathbf{q}), \tag{2}$$

where A is the area of the sample, μ is the chemical potential, $V(\mathbf{q})=2\pi e^2/\epsilon q$ is the Coulomb interaction in graphene ($\epsilon\sim 2-5$), and

$$\hat{\rho}^{\sigma,\sigma'}_{n,n'}(\mathbf{q}) = \frac{1}{N_\phi}\sum_{k,k'} e^{-i/2q_x(k+k')l_B^2}\delta_{k,k'-q_y}c^\dagger_{nk\sigma}c_{n'k'\sigma'}, \tag{3}$$

with $c^\dagger_{nk\sigma}(c_{nk\sigma})$ representing the creation (annihilation) operator for state $|n,k,\sigma\rangle$. Equation (3) is related to the density matrix operator in the momentum space,

$$\hat{\rho}(\mathbf{q}) = \sum_{nn'\sigma\sigma'} \mathcal{F}_{n,n'}(-\mathbf{q})\hat{\rho}^{\sigma,\sigma'}_{n,n'}(\mathbf{q}), \tag{4}$$

where the form factor for graphene (with $n,n'\geq 0$) is given by[10]

$$\mathcal{F}_{n,n'}(\mathbf{q}) = \delta_{n,0}\delta_{n',0}F_{0,0}(\mathbf{q}) + \frac{1}{\sqrt{2}}\delta_{nn',0}(1-\delta_{n+n',0})F_{n,n'}(\mathbf{q}) + \frac{1}{2}(1-\delta_{nn',0})[F_{n,n'}(\mathbf{q})+F_{n-1,n'-1}(\mathbf{q})]. \tag{5}$$

We recall that $\mathcal{F}_{n,n'}(\mathbf{q})$ is a linear combination of the form factors for a conventional 2D system,[10]

$$F_{n\geq n'}(\mathbf{q}) = \sqrt{\frac{n'!}{n!}}\left[\frac{(iq_x-q_y)}{\sqrt{2}}\right]^{(n-n')} L_n^{(n-n')}\left(\frac{q^2}{2}\right)e^{-q^2/4}, \tag{6}$$

where $L_n^m(x)$ is the generalized Laguerre polynomial and $F_{n\leq n'}(\mathbf{q})=F^*_{n',n}(-\mathbf{q})$.

The derivation of the mean-field Hamiltonian using Hartree–Fock approximation is straightforward[13] and gives

$$\hat{H}_{\mathrm{HF}} = N_\phi \sum_{\sigma n}(E_n-\mu)\hat{\rho}^{\sigma,\sigma}_{n,n}(0) + N_\phi \sum_{\sigma_i n_j \mathbf{q}} U_{\sigma_1 n_1,\sigma_2 n_2}(\mathbf{q})\hat{\rho}^{\sigma_1,\sigma_2}_{n_1,n_2}(\mathbf{q}), \tag{7}$$

where $U_{\sigma_1 n_1,\sigma_2 n_2}(\mathbf{q})=H_{\sigma_1 n_1,\sigma_2 n_2}(\mathbf{q})-X_{\sigma_1 n_1,\sigma_2 n_2}(\mathbf{q})$. The self-consistent electrostatic and exchange potentials are given by

$$H_{\sigma_1 n_1,\sigma_2 n_2}(\mathbf{q}) = \delta_{\sigma_1,\sigma_2}\sum_{n_3 n_4 \sigma} H_{n_1 n_3,n_2 n_4}(\mathbf{q})\rho^{\sigma,\sigma}_{n_3,n_4}(-\mathbf{q}), \tag{8}$$

$$X_{\sigma_1 n_1,\sigma_2 n_2}(\mathbf{q}) = \sum_{n_3 n_4} X_{n_1 n_3,n_2 n_4}(\mathbf{q})[\delta_{\sigma_1,\sigma_2}\rho^{\sigma_1,\sigma_1}_{n_3,n_4}(-\mathbf{q}) + \delta_{\sigma_1,\bar{\sigma}_2}\rho^{\sigma_1,\sigma_1}_{n_3,n_4}(-\mathbf{q})], \tag{9}$$

where

$$H_{n_1 n_3,n_2 n_4}(\mathbf{q}) = \frac{1}{2\pi l_B^2}V(\mathbf{q})(1-\delta_{\mathbf{q},0})\mathcal{F}_{n_1,n_2}(-\mathbf{q})\mathcal{F}_{n_3,n_4}(\mathbf{q}), \tag{10}$$

$$X_{n_1 n_3,n_2 n_4}(\mathbf{q}) = \int \frac{d\mathbf{k}}{(2\pi)^2}V(\mathbf{k})e^{-il_B^2\mathbf{k}\times\mathbf{q}\cdot\hat{z}}\mathcal{F}_{n_1,n_4}(\mathbf{k})\mathcal{F}_{n_3,n_2}(-\mathbf{k}), \tag{11}$$

and $\rho^{\sigma_1,\sigma_2}_{n_1,n_2}(\mathbf{q})=\langle\hat{\rho}^{\sigma_1,\sigma_2}_{n_1,n_2}(\mathbf{q})\rangle$ are the density matrix elements, which should be self-consistently determined from Eq. (7). The density matrix is obtained from the equal-time limit $(\tau\to 0^-)$ of the single-particle Green's function,

$$G^{\sigma_1,\sigma_2}_{n_1,n_2}(k_1,k_2;\tau) = -\langle \mathrm{T}c_{n_1 k_1 \sigma_1}(\tau)c^\dagger_{n_2 k_2 \sigma_2}(0)\rangle. \tag{12}$$

The equation of motion for the Green's function in Fourier space is given by[10]

$$\delta_{\sigma_1,\sigma_2}\delta_{n_1,n_2}\delta_{\mathbf{q},0} = [i\omega_n-(E_{n_1}-\mu)]G^{\sigma_1,\sigma_2}_{n_1,n_2}(\mathbf{q},i\omega_n) - \sum_{\sigma_3 n_3 \mathbf{q}'}\Sigma_{\sigma_1 n_1,\sigma_3 n_3}(\mathbf{q},\mathbf{q}')G^{\sigma_3,\sigma_2}_{n_3,n_2}(\mathbf{q}',i\omega_n) \tag{13}$$

and the Hartree–Fock self-energy matrix is $(\mathbf{p}=\mathbf{q}-\mathbf{q}')$

$$\Sigma_{\sigma_1 n_1,\sigma_3 n_3}(\mathbf{q},\mathbf{q}') = \sum_{m_1 m_3}\{[H_{n_1 m_1,n_3 m_3}(-\mathbf{p})\rho_{m_3,m_1}(\mathbf{p}) - X_{n_1 m_1,n_3 m_3}(-\mathbf{p})\rho^{\sigma_1,\sigma_1}_{m_3,m_1}(\mathbf{p})]\delta_{\sigma_1,\sigma_3} - X_{n_1 m_1,n_3 m_3}(-\mathbf{p})\rho^{\bar{\sigma}_1,\sigma_1}_{m_3,m_1}(\mathbf{p})\delta_{\sigma_3,\bar{\sigma}_1}\}e^{i/2l_B^2\mathbf{q}\times\mathbf{q}'\cdot\hat{z}}, \tag{14}$$

where we have defined $\rho_{m_3,m_1}(\mathbf{p})=\Sigma_\sigma\rho^{\sigma,\sigma}_{m_3,m_1}(\mathbf{p})$.

In the SLLA for the nth level, all Landau-level indices in Eq. (13) are the same, $n_1=n_2=n_3=n$. To account for the inter-Landau-level transitions, we restrict the indices to n and $n+1$. The Green's function in the Landau-level space then becomes a 2×2 matrix,

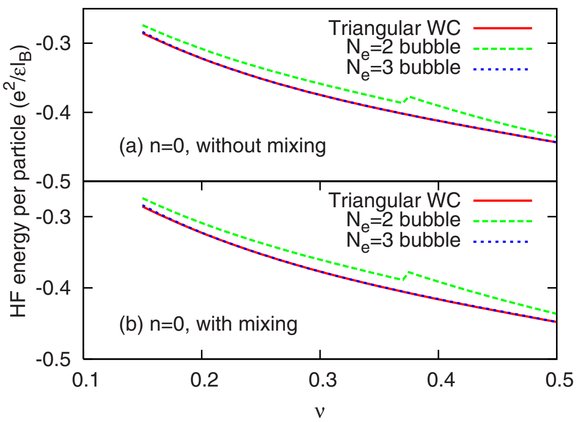

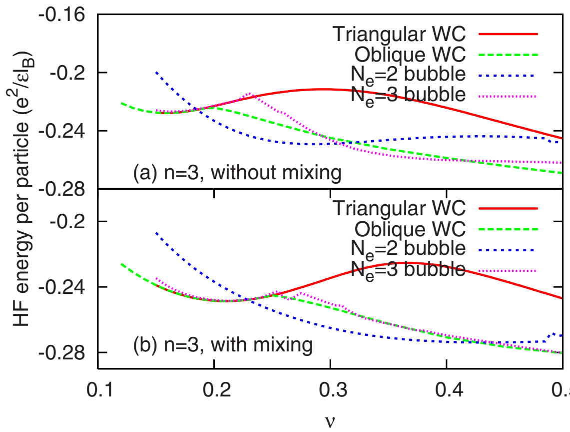

FIG. 1. (Color online) Ground state energy per particle, measured in units of $e^2/\epsilon l_B$, for different crystal structures in the $n=0$ (left) and $n=3$ (right) Landau levels in graphene. The top panel (a) shows results without Landau-level mixing, whereas the bottom panel (b) shows results with mixing. We see that, in each case, the *ground state energy* is lowered due to Landau-level mixing (Ref. 17). Note that the $n=0$ phase diagram is qualitatively unchanged, whereas for $n=3$, the bubble phase with $N_e=3$ electrons disappears when Landau-level mixing is taken into account.

$$\tilde{G}^{\sigma_1,\sigma_2}(\mathbf{q},i\omega_n)=\begin{bmatrix} G^{\sigma_1,\sigma_2}_{n,n} & G^{\sigma_1,\sigma_2}_{n,n+1} \\ G^{\sigma_1,\sigma_2}_{n+1,n} & G^{\sigma_1,\sigma_2}_{n+1,n+1}\end{bmatrix}(\mathbf{q},i\omega_n) \tag{15}$$

and similarly, the self-energy matrix $\tilde{\Sigma}_{\sigma_1,\sigma_2}(\mathbf{q},\mathbf{q}')$ is a 2×2 matrix in the Landau-level space. The equation of motion for the Green's function [Eq. (13)] becomes

$$\delta_{\sigma_1,\sigma_2}\delta_{\mathbf{q},0}=[i\omega+\mu]\tilde{G}^{\sigma_1,\sigma_2}(\mathbf{q},i\omega_n)-\sum_{\sigma_3\mathbf{q}'}[\tilde{\Sigma}_{\sigma_1,\sigma_3}(\mathbf{q},\mathbf{q}') + \tilde{E}\delta_{\mathbf{q},\mathbf{q}'}\delta_{\sigma_1,\sigma_3}]\tilde{G}^{\sigma_3,\sigma_2}(\mathbf{q}',i\omega_n), \tag{16}$$

where the kinetic energy matrix in the Landau-level space is diagonal, $\tilde{E}=\mathrm{diag}(E_n,E_{n+1})$. We solve Eq. (16) by obtaining the eigenvalues and eigenvectors

$$\sum_{\sigma_3\mathbf{q}'}[\tilde{\Sigma}_{\sigma_1,\sigma_3}(\mathbf{q},\mathbf{q}')+\tilde{E}\delta_{\mathbf{q},\mathbf{q}'}\delta_{\sigma_1,\sigma_3}]\tilde{V}_{\sigma_3}(\mathbf{q}',k)=\omega_k\tilde{V}_{\sigma_1}(\mathbf{q},k). \tag{17}$$

Here, $\tilde{V}^{\dagger}_{\sigma}(\mathbf{q},k)=[V^{*}_{\sigma,n}(\mathbf{q},k),V^{*}_{\sigma,n+1}(\mathbf{q},k)]$ is the eigenvector with the eigenvalue ω_k. We can construct the self-consistent mean-field Green's function using these eigenvectors,[10]

$$\tilde{G}^{\sigma_1,\sigma_2}(\mathbf{q},i\omega_n)=\sum_k \frac{\tilde{V}_{\sigma_1}(\mathbf{q},k)\tilde{V}^{\dagger}_{\sigma_2}(0,k)}{i\omega_n-\omega_k+\mu}, \tag{18}$$

which, in turn, leads to the self-consistent density matrix

$$\rho^{\sigma_1,\sigma_2}_{n_1,n_2}(\mathbf{q})=\sum_k V_{\sigma_2,n_2}(\mathbf{q},k)V^{*}_{\sigma_1,n_1}(0,k)f(\omega_k-\mu), \tag{19}$$

where $f(x)=\theta(-x)$ denotes the Fermi function at zero temperature. The chemical potential μ is determined by the constraint that the total occupation in the two Landau levels is equal to the partial filling factor,

$$\sum_{\sigma}[\rho^{\sigma,\sigma}_{n,n}(0)+\rho^{\sigma,\sigma}_{n+1,n+1}(0)]=\nu. \tag{20}$$

By using the self-consistent density matrix (19), we calculate the Hartree–Fock mean-field energy E_{HF} for various trial lattice configurations to obtain the ground state crystal structure.

III. RESULTS

We consider mean-field Wigner crystal lattices with two primitive lattice vectors $\mathbf{a}_1=(a,b/2),\mathbf{a}_2=(0,b)$ and define the lattice anisotropy as $\gamma=b/a$. Note that the triangular lattice ($\gamma=2/\sqrt{3}=1.15$) and quasistriped states ($\gamma\to 0$) are special cases of the general anisotropic lattice that is defined by these primitive vectors. The lattice constants a and b are determined by the constraint that a unit cell contains N_e electrons, and are given by $a=l_B\sqrt{2\pi N_e/\nu\gamma}$ and $b=a\gamma$. The reciprocal lattice vectors are $\mathbf{Q}_{mn}=m\mathbf{b}_1+n\mathbf{b}_2$, where $\mathbf{b}_1=(2\pi/a)(1,0)$ and $\mathbf{b}_2=(2\pi/a)(-1/2,1/\gamma)$ are the reciprocal lattice basis vectors. We determine the optimal lattice structure by choosing the γ ($0<\gamma\le 2/\sqrt{3}$) and N_e that minimize the mean-field energy E_{HF}. In the following, we denote crystals with one electron per unit cell, $N_e=1$, as Wigner crystals and those with $N_e\ge 2$ per unit cell as bubble crystals.[14,16] We first calculate the self-consistent density matrix without Landau-level mixing, $\rho^{\sigma_1,\sigma_2}_{n,n}(\mathbf{q})\neq 0$ and $\rho^{\sigma_1,\sigma_2}_{n+1,n}(\mathbf{q})=0=\rho^{\sigma_1,\sigma_2}_{n+1,n+1}(\mathbf{q})$. We then use that matrix as the initial point for the density matrix with Landau-level mixing.

Figure 1 shows the mean-field energy per particle for various lattice structures as a function of ν for Landau level $n=0$ (left) and $n=3$ (right). We note that the *ground state energy* for a given ν is lowered by the Landau-level mixing, as expected from the perturbation theory.[17] For $n=0$, we find that a triangular Wigner crystal is the mean-field ground state with or without Landau level mixing. For $n=3$, we find that the triangular lattice remains a ground state for higher values of ν when the inter-Landau-level mixing is taken into ac-

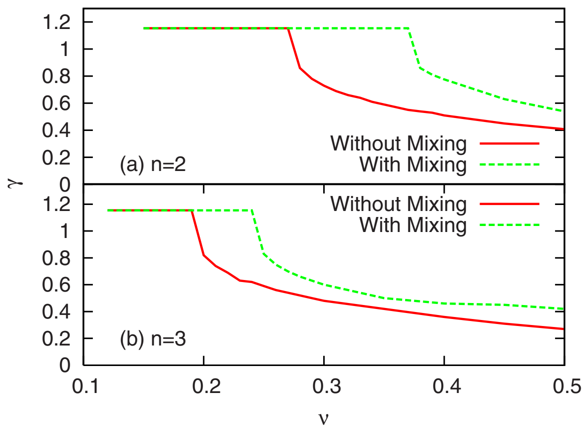

FIG. 2. (Color online) Ground state lattice anisotropy $\gamma(\nu)$ in graphene for $n=2$ (top) and $n=3$ (bottom) Landau levels. The solid (red) line shows the result without mixing and the dashed (green) line indicates the result with Landau-level mixing. $\gamma=2/\sqrt{3}=1.15$ corresponds to a triangular lattice whereas $\gamma\leq 0.5$ corresponds to highly anisotropic Wigner crystals or quasistriped states.

count and that the $N_e=3$ bubble phase vanishes from the ground state.

The most visible effect of inter-Landau-level mixing is the systematic up-shift of critical values of ν at which transitions from one crystal structure to another occur. For example, at $n=3$, the transition from an isotropic Wigner crystal to an $N_e=2$ anisotropic bubble state occurs at $\nu\sim 0.20$ without Landau-level mixing; this critical value is shifted upward to $\nu\sim 0.25$ when the mixing is taken into account (Fig. 1). This shift is also visible in the lattice anisotropy $\gamma(\nu)$ for the ground state crystal structure, as shown in Fig. 2. At small ν, the lattice is triangular and $\gamma=2/\sqrt{3}=1.15$ is a constant. At higher values of ν, the anisotropy increases, leading to a quasistriped structure for the ground state. We see from Fig. 2 that the region of stability of the triangular lattice increases when inter-Landau-level transitions are taken into account. This result is consistent with the classical expectations. As the Landau-level mixing increases, it is possible to create wave packets that are localized on length-scales shorter than l_B, approaching, eventually, a δ-function wave packet when the mixing from all Landau levels is considered. Therefore, the region of stability of a triangular Wigner crystal, which is the ground state for a classical problem, increases when Landau-level mixing is taken into account.

Results in Figs. 1 and 2 suggest that the effect of Landau-level mixing is not dominant in higher Landau levels, even though the energy gap between adjacent Landau levels becomes smaller. To understand this unexpected result, we recall that the inter-Landau-level transitions from $n\to n+1$ are determined by the off-diagonal self-energy matrix elements and the gap between adjacent Landau levels, $\Sigma_{\sigma n,\sigma n+1}/\Delta E_n$. It follows from Eqs. (14), (10), and (11) that for large n,

$$\Sigma_{\sigma n,\sigma n+1} \sim \frac{\rho^{\sigma,\sigma}_{n,n+1}}{(n+1)} + \frac{a\rho^{\sigma,\sigma}_{n,n} + b\rho^{\sigma,\sigma}_{n+1,n+1}}{\sqrt{n+1}} \tag{21}$$

because $\mathcal{F}_{n,n+1}\sim 1/\sqrt{n+1}$. We find that this asymptotic behavior is reproduced by our results. We quantify the Landau-level mixing by the ratio of relative occupations of the two levels in question, ρ_{n+1}/ρ_n, where $\rho_m=\Sigma_\sigma \rho^{\sigma,\sigma}_{m,m}(0)$. The left panel in Fig. 3 shows the ratio $\Sigma_{n,n+1}/\Delta E_n$ as a function of Landau level index n for graphene (solid red) and the conventional 2D system (dotted green) at partial filling factor $\nu=0.5$. We see that the ratio $\Sigma_{\sigma n,\sigma n+1}(0,\mathbf{Q}_{01})/\Delta E_n$, for typical off-diagonal self-energy matrix elements in graphene, is smaller than 4%. In contrast to this, the ratio and the self-energy for a conventional 2D system monotonically decreases since $\Delta E_n=\hbar\omega_c$ is independent of n and is well described by a $1/\sqrt{n+1}$ dependence at large n. We recall that this ratio for a conventional 2D system depends on the magnetic field B or the magnetic length l_B. Our results are for $g=l_B/a_B=0.67$ or $l_B\sim 35$ Å. (This $g=V_c/\Delta E_n$ for a conventional 2D system is equal to the $g=\alpha_G$ in graphene with $\epsilon=3.3$ as the dielectric constant.) The right panel in Fig. 3 shows the corresponding relative occupations for graphene (solid red) and the conventional 2D system (dotted green). The fact that this ratio, in the presence of inter-Landau-level mixing, is small $(\rho_{n+1}/\rho_n\leq 4\%)$ provides complementary support for the validity of SLLA in graphene.

IV. DISCUSSION

In this paper, we have investigated the effects of inter-Landau-level transitions on Wigner crystal mean-field states

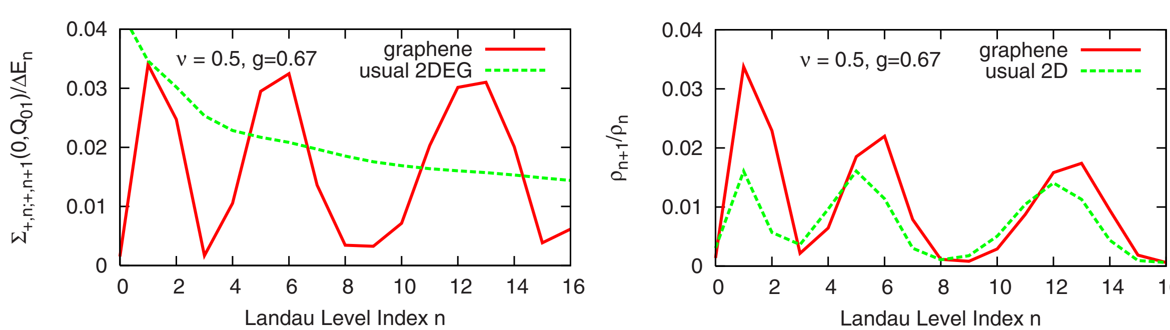

FIG. 3. (Color online) Left: $\Sigma_{+,n;+,n+1}/\Delta E_n$ as a function of n for partial filling factor $\nu=0.5$ in graphene (solid red) and a conventional 2D system (dotted green). In graphene, the ratio is small for all n and shows that SLLA is applicable even in high Landau levels when $\Delta E_n\to 0$. In conventional 2D systems, the ratio monotonically decays as $1/\sqrt{n+1}$ for large n. Right: Corresponding ratio of occupation numbers ρ_{n+1}/ρ_n for graphene (solid red) and conventional 2D system (dotted green) provides further support for the validity of SLLA in high Landau levels.

in graphene obtained using single-Landau-level approximation.[10] Our results show that the Landau-level mixing does not qualitatively change the phase diagram of the system, although it shifts upward the critical values of filling factor ν at which transitions from one lattice structure to another occur. We quantify the Landau-level mixing in terms of off-diagonal self-energy and relative occupation numbers, and show that it remains small as a function of the Landau-level index n. Thus, we conclude that SLLA provides a reliable description of Wigner crystal ground states in graphene.

We emphasize that our results for graphene are independent of the magnetic field B. For conventional 2D systems, the Landau-level mixing depends on the magnetic field and can be important at weak fields $B \leq B_c$ when the magnetic length becomes larger than the Bohr radius of the massive carriers, $l_B \geq a_B$ for $B \leq B_c$. The absence of a corresponding critical field B_c in graphene is due to the massless nature of the carriers. Our conclusions do not depend, qualitatively, on the range of the interaction $V(\mathbf{q})$ because the large-q scattering is strongly suppressed by the form factors $\mathcal{F}(\mathbf{q})$ that exponentially decay with q. In this paper, we have ignored transitions to next-higher Landau levels[13] $n \to n+k$ because the amplitude for them rapidly vanishes: $\Sigma_{n,n+k}/\Delta E_{nk} \sim \sqrt{(n+1)!/(n+k)!k^2} \to 0$ as $n \to \infty$ for $k \geq 2$. This estimate follows from an analysis similar to that for Eq. (21) and the observation that, in graphene, $\Delta E_{nk} = E_{n+k} - E_n \propto k/\sqrt{n}$ for large $n \gg k$. Therefore, it is sufficient to consider the Landau-level mixing only between adjacent levels.

Since carriers in graphene are on the surface, in contrast to those in the conventional 2D system, it is an ideal candidate for *direct observation of the local carrier density structure*.[9] Our results provide further support for the existence of triangular Wigner lattice as the ground state at small ν and anisotropic ground states in high Landau levels for $\nu \to 1/2$.[10,11] A direct observation of carrier density in graphene in the quantum Hall regime will verify (or falsify) our conclusions.

ACKNOWLEDGMENTS

This work was supported by Research Support Funds Grant from the IUPUI.

1. E. Wigner, Phys. Rev. **46**, 1002 (1934).
2. A. L. Fetter and J. D. Walecka, *Quantum Theory of Many-Particle System* (Dover, New York, 2003).
3. B. Tanatar and D. M. Ceperley, Phys. Rev. B **39**, 5005 (1989).
4. H. A. Fertig, in *Perspectives in Quantum Hall Effects*, edited by S. Das Sarma and A. Pinczuk (Wiley, New York, 1997).
5. R. L. Willett, H. L. Stormer, D. C. Tsui, L. N. Pfeiffer, K. W. West, and K. W. Baldwin, Phys. Rev. B **38**, 7881 (1988).
6. M. P. Lilly, K. B. Cooper, J. P. Eisenstein, L. N. Pfeiffer, and K. W. West, Phys. Rev. Lett. **82**, 394 (1999).
7. H. A. Fertig, Phys. Rev. Lett. **82**, 3693 (1999); A. H. MacDonald and M. P. A. Fisher, Phys. Rev. B **61**, 5724 (2000).
8. K. S. Novoselov, A. K. Geim, S. V. Morozov, D. Jiang, M. I. Katsnelson, I. V. Grigorieva, S. V. Dubonos, and A. A. Firsov, Nature (London) **438**, 197 (2005); Y. Zhang, Y.-W. Tan, H. L. Stormer, and P. Kim, *ibid.* **438**, 201 (2005).
9. J. Martin, N. Akerman, G. Ulbricht, T. Lohmann, J. H. Smet, K. von Klitzing, and A. Yacobi, Nat. Phys. **4**, 144 (2008).
10. C.-H. Zhang and Y. N. Joglekar, Phys. Rev. B **75**, 245414 (2007).
11. Hao Wang, D. N. Sheng, L. Sheng, and F. D. M. Haldane, Phys. Rev. Lett. **100**, 116802 (2008).
12. The band mass of carriers is $m \sim 0.4m_e - 0.05m_e$ where m_e is the bare electron mass. It depends on the semiconductor heterojunction and the polarity of the carriers (electrons are lighter than holes in a given heterojunction if it supports both type of carriers). See M. E. Cage, in *The Quantum Hall Effects*, edited by R. E. Prange and S. M. Girvin (Springer, New York, 1990).
13. A. H. MacDonald, Phys. Rev. B **30**, 4392 (1984).
14. M. O. Goerbig, P. Lederer, and C. M. Smith, Phys. Rev. B **69**, 115327 (2004).
15. M. O. Goerbig and C. Morais Smith, Europhys. Lett. **63**, 736 (2003).
16. A. A. Koulakov, M. M. Fogler, and B. I. Shklovskii, Phys. Rev. Lett. **76**, 499 (1996).
17. J. J. Sakurai, *Modern Quantum Mechanics* (Addison-Wesley, Reading, MA, 1995).